CDF/ANAL/TOP/CDFR/9733
Draft 0.1
April 6, 2009

An Inclusive Dilepton Analysis using 3 fb^{-1}

M. Stephen M. Smith, Douglas Benjamin, Mark C. Kruse
Duke University

Dean Andrew Hidas
Rutgers University

Abstract

We present results using 3.0fb^{-1} of CDF data from a global fitting method to high-P_T $e\mu$ events. This method was developed earlier in Run 2 using 200pb^{-1}, by the same group as the present analysis, and published in PRD [1]. This method was dubbed "AIDA" (An Inclusive Dilepton Analysis) in that first analysis. The method uses a $\not\!\!E_T$-N_{jet} parameter space that allows for a very nice separation of the main processes ($t\bar{t}$, WW and $Z \to \tau\tau$) that make up the $e\mu$ sample.

Here we extend the previous method for the extraction of the $t\bar{t}$, WW and $Z \to \tau\tau$ cross sections, and develop a quantitative likelihood for the consistency of the data to the SM hypothesis in this parameter space.

In using this method for the extraction of cross sections, our measurements using 3.0fb^{-1} of $e\mu$ data are: $\sigma_{t\bar{t}} = 8.20^{+1.17}_{-1.07}$ pb, $\sigma_{WW} = 12.28^{+2.05}_{-1.87}$ pb, and $\sigma_{Z\to\tau\tau} = 1513^{+173}_{-159}$ pb.

As a result of no events being lost from event cuts after the requirement of 2 high-P_T leptons, these results are competitive with the respective dedicated analyses, albeit only using $e\mu$ events.

The results of quantifying the consistency of the data to the SM hypothesis yield no significant deviations from SM expectations. Although not done in this iteration of the analysis, this technique could also be used to search for specific new physics dilepton signatures.

Contents

1 Introduction **3**
1.1 Main differences from previous analysis 5

2 Event Selection **5**
2.1 Datasets and Luminosity 6
2.2 Monte Carlo datasets 6
2.3 Lepton ID 7
2.4 Dilepton Selection 9

3 Signal and Background acceptances **10**

4 Data and grand summary of expectations **11**

5 Parameter space distributions for data and MC **11**

6 The Likelihood fit technique **15**
6.1 Pseudo-experiments 16

7 Systematics **19**
7.1 Acceptance systematics 19
7.2 Shape systematics 20

8 Fit results **21**

9 Likelihood of Standard Model hypothesis **21**

10 Summary and possible future improvements **26**

1 Introduction

This analysis was developed as a more global means of understanding the content of the high-P_T dilepton sample. After the requirement of 2 high-P_T leptons only, we consider the processes that can make up this sample and ask the question what other objects can exist in these events. The answer is neutrinos (which give $\not\!\!E_T$) and jets (either from decays of final state objects, or from initial or final state radiation). So the most straightforward thing to do is simply fit the $\not\!\!E_T$ vs. N_{jet} 2-D distribution from the data to those from the expected SM contributions, to extract the cross sections from these contributions. This works extremely well because of a very nice feature of this sample: the main contributions appear in very different regions of the $\not\!\!E_T$ vs. N_{jet} parameter space because of their different sources of $\not\!\!E_T$ and jets.

This method was first performed on 200pb^{-1} of data [1, 2]. The results from this dilepton study was the extraction of the $t\bar{t}$, WW, and the $Z \to \tau\tau$ cross-sections, in an independent and more inclusive way to the counting experiment analyses.

Here, we repeat this measurement using 3.0fb^{-1} with the differences discussed below in section 1.1. In the present analysis we only use the $e\mu$ dilepton events.

The main processes that contribute to the $e\mu$ channel are WW, $Z \to \tau\tau$ and $t\bar{t}$, and it is for these processes we want to extract cross sections. Additionally we have a fake lepton contribution in $W + jet$ and $W\gamma$ events, and also WZ and ZZ contributions. We also have a relatively significant contribution from $Z \to \mu\mu$ events where one of the muons has radiated a high-E_T photon which, together with the muon track, gives an electron signature. These latter smaller contributions we fix [1] in all our fits, normalized to their expected values for a given integrated luminosity. We allow the cross sections of our main signals (WW $Z \to \tau\tau$ and $t\bar{t}$) to float in the fit. The fit technique is explained in more detail in section 6.

Besides electrons and muons in all of these sources, the only other objects are jets and neutrinos. We maximally exploit this fact by not cutting on variables related to these objects, but rather fitting the data in the 2-D $\not\!\!E_T$-N_{jet} and $\not\!\!E_T$-$\sum E_T(jets)$ parameter spaces to the expected sources.

A nice feature of this approach lies in the very different regions of $\not\!\!E_T$-N_{jet} space occupied by the relatively few SM processes contributing to the high-P_T $e\mu$ sample. This is illustrated schematically in Figure **??**. Specifically, for the $e\mu$ channel:

1 $t\bar{t}$:
The jets in the event primarily come from b quarks from the top decay. There can also be a contribution from ISR and FSR. This gives a jet multiplicity peak around 2 jets. The $\not\!\!E_T$ in the event comes from leptonic W decay. The $\not\!\!E_T$ is not very correlated to the jet multiplicity.

2 WW:
The jets in the event come from ISR and FSR only. This implies a steeply

[1] As will be explained later, we use the term "fix" as synonymous with "Gaussian constrain".

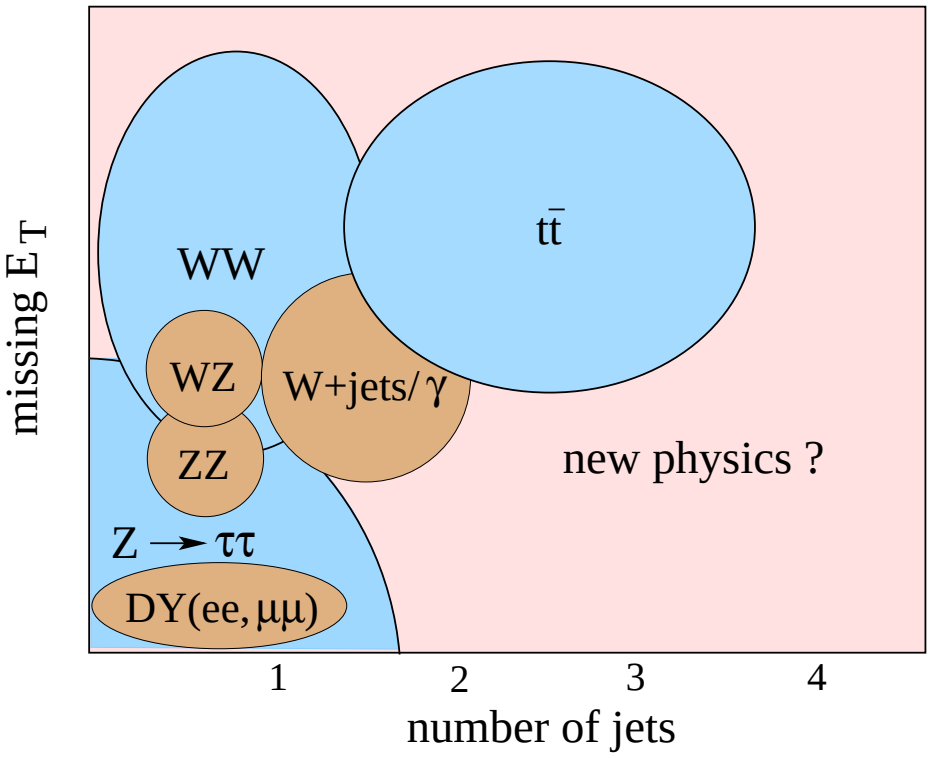

Figure 1: Schematic of the various $e\mu$ sources in the $\not\!\!E_T$-N_{jet} parameter space.

falling jet multiplicity spectrum. The $\not\!\!E_T$ comes from W decays and is typically much larger than for $Z \to \tau\tau$. Also the $\not\!\!E_T$ is somewhat correlated to the jet multiplicity.

3 $Z \to \tau\tau$:
The jets in the event come from ISR and FSR only. This implies a steeply falling jet multiplicity spectrum. The $\not\!\!E_T$ comes from the τ decays, and is strongly correlated to the jet multiplicity: the $\not\!\!E_T$ tends to be close to zero with no jets in the events, but when the Z recoils off ISR the neutrino directions are more aligned and the $\not\!\!E_T$ increases significantly.

4 Other contributions: (to be fixed to expected number of events):
The $b\bar{b}$ contribution is expected to be small with very small $\not\!\!E_T$. The fake contribution (from mis-identifying jets as leptons), is expected to have a steeply falling jet multiplicity, but significant $\not\!\!E_T$ from the W decay. ...

Once we obtain both the MC distributions and the data distributions in the parameter spaces, we proceed to fit the data to the SM contributions as described in section 6 using a maximum likelihood method.

From our likelihood fit of the data to a combination of the 3 main SM processes, our main objectives here are:

1 Measure the $t\bar{t}$, WW, and $Z \to \tau\tau$ cross sections. We gain significant statistical power using this technique as we make no other cuts besides lepton selection, however, we also only use $e\mu$ events which reduces our statistics somewhat. We can extract all the cross sections simultaneously from a single fit. However, we will also present the $t\bar{t}$, WW, and $Z \to \tau\tau$ cross-sections by fixing (within Gaussian constraints) every other contribution to their expected values.

2 Test the consistency of the high-P_T dilepton sample to the SM hypothesis. To do this we allow the various SM contributions to float in the fit, and extract a likelihood value which we then compare with pseudo-experiments composed solely of SM processes (using our expected contributions from those processes). This by itself is not very optimal in looking for deviations from the SM as the likelihood will be driven by the high statistics regions of the parameter space, so what we do is break up the parameter space into sectors and derive separate likelihoods for each sector. It future iterations this could be better refined.

1.1 Main differences from previous analysis

The main differences between this analysis and the previous incarnation [2] are as follows:

- Here we only use the $e\mu$ dilepton category for simplicity to avoid the previous complications in dealing with the Drell-Yan background. In CDF-6870 ee and $\mu\mu$ events were included but at the expense of having to deal with these categories in a non-uniform manner (an additional $\not\!\!E_T$-significance cut had to be added to the dilepton selection).
- We use the same $e\mu$ categories as used in the $H \to WW$ analysis [3], which differ (have greater coverage) from CDF-6870.
- We explore using the $\not\!\!E_T$-$\sum E_T(jets)$ parameter space in addition to $\not\!\!E_T$-N_{jet}. The rational being that using $\sum E_T(jets)$ will result in greater separation of $t\bar{t}$ (where the jets come from final-state b-quarks) from WW and $Z \to \tau\tau$ (where the jets come from QCD radiation).
- We extend the method to quantify the consistency of the data to the SM hypothesis. We do this in different sectors of the parameter space. This is discussed further in section 9.

2 Event Selection

The dilepton selection we use here is based on that from our recent $H \to WW$ analysis [3]. We use a subset of the dilepton categories used in that analysis (here we only

Good run list	$\int \mathcal{L}dt$ (pb^{-1})
EM_NOSI	2960.5
EM_CMUP_NOSI	2922.9
EM_MU_NOSI_CMXIGNORED	2829.5
EM_SI	2820.5
EM_CMUP_SI	2785.4
EM_MU_SI_CMXIGNORED	2695.4

Table 1: Luminosity corresponding to the different good run lists (v23) used in this analysis.

use $e\mu$ events) and exactly the same lepton definitions and much of the same analysis code. We refer the reader to that note (CDF-9697) for details of the lepton ID cross checks by measuring the Z cross sections for the various lepton categories, and several other cross checks including that from same-sign events (which agrees very well with expectations) and other control region checks.

Below we summarize the main event selection relevant to this analysis.

2.1 Datasets and Luminosity

We use the high-P_T single lepton trigger paths:

- ELECTRON_CENTRAL_18
- MUON_CMUP_18
- MUON_CMX_18

The corresponding datasets are bhel0d/0h/0i/0j/0k/0m (electrons) and bhmu0d/0h/0i/0j/0k/0m (muons). The good run lists we use are given in Table 1 together with their respective integrated luminosities.

2.2 Monte Carlo datasets

The signal acceptances and several of the backgrounds are estimated using Monte Carlo samples. Table 2 lists all the samples used. Here we provide some brief notes on the samples. More details of these samples can be found in reference [3].

$t\bar{t}$: We use a $t\bar{t}$ PYTHIA sample generated at a mass of 175 GeV, using Gen5 for the full run range and with no minbias in the events.

WW : We use a NLO Monte Carlo generator, MC@NLO. Both W's required to decay to e, μ, or τ

mode	Period	MC dataset	MC events generated	Stntuple	$\sigma \times BR$ (pb)	K-factor[a]	Filter Eff
$W\gamma \to e\nu\gamma$	0-11	rewk68	9253090	re0s68	13.6×1.36	1.36	1.0
$W\gamma \to \mu\nu\gamma$	0-11	rewk69	8847641	re0s69	13.6×1.36	1.36	1.0
$W\gamma \to \tau\nu\gamma$	0-11	rewk6a	8963142	re0s6a	13.6×1.36	1.36	1.0
WW	0-17	wewk5d,wewkbd,wewkgd wewkkd,wewknd,wewkaf wewkgf	19408712	we0s5d,we0sbd,we0sgd we0skd,we0snd,we0saf we0sgf	1.27	1.0	1.0
WW@NLO	0-7	wewkfd,wewked	1361835	we0sfd,we0sed	1.27	1.0	1.0
WZ	0-17	wewk6d,wewkcd,wewkhd wewkld,wewkod,wewkbf wewkhf	20249606	we0s6d,we0scd,we0shd we0sld,we0sod,we0sbf we0shf	0.365	1.0	0.76
ZZ	0-17	wewk7d,wewkdd,wewkid wewkmd,wewkpd,wewkcf wewkif	19352335	we0s7d,we0sdd,we0sid we0smd, we0spd,we0scf we0sif	1.511	1.0	0.23
$t\bar{t}$	0-11	tewk2z	1813748	te0s2z	6.7×0.1026	1.0	1.0
$Z \to ee$	0-17	zewk6d,zewkad,zewkcd zewkdd,zewked,zewkee zewkeh,zewkej,zewkei	31228108	ze1s6d[b],ze1sad,ze0scd ze0sdd,ze0sed,ze0see ze0seh, ze0sej,ze0sei	355	1.4	1.0
$Z \to \mu\mu$	0-17	zewk6m,zewk9m,zewkbm zewkcm,zewkdm,zewkem zewkfm,zewkgm,zewkim	31187751	ze1s6m[b],ze1s9m,ze0sbm ze0scm,ze0sdm,ze0sem ze0sfm, ze0sgm,ze0sim	355	1.4	1.0
$Z \to \tau\tau$	0-11	zexoet	1542579	zx0set	1272[c]	1.4	0.00713

[a] If cross-section is NLO then K-factor is one.
[b] Gen5 tarball for period 0 [c] $m_{ll} > 10$

Table 2: Monte Carlo samples used in this analysis

$Z/\gamma^* \to \tau\tau$: A PYTHIA sample is used with a 10 GeV minimum dilepton mass, and which uses Gen5 for the full run range and has no minbias in the events.

WZ/ZZ : We use PYTHIA samples. The WZ samples are decayed with the Z decaying to a pair e, μ, or τ, and the W decaying inclusively, which is then filtered for two leptons above 1 GeV. The ZZ sample is constructed with both Z's decaying inclusively and then filtered for two leptons above 1 GeV. The ZZ Monte Carlo has a γ^* component in it and has an $M_{ll} > 15$ GeV generator level requirement.

$W\gamma$: The $W\gamma$ Monte Carlo used for this analysis uses the Baur matrix element generator [4] which is passed to PYTHIA via the LesHouchesModule.

$Z \to ee/\mu\mu$: These PYTHIA samples are generated with a 20 GeV minimum dilepton mass. They use Gen5 for the 0d run range and Gen6 for the 0h/0i/0j/0k run range. They have a full luminosity dependent addition of minbias in the events.

2.3 Lepton ID

The lepton identification requirements are identical to those detailed in CDF-9697 [3], though not all the lepton categories used in that analysis are used here.

Electrons identified as Tight Central Electron (TCE) and forward (PHX) are used in this analysis. A central or TCE electron is identified in the $|\eta|$¡1.1 region of the detector while a PHX or forward electron is identified in the 1.1¡$|\eta|$¡2.0 region of the detector. The ID requirements are summarize in Table **??**.

Central Electrons (TCE)	
Region	Central ($\|\eta\|$ <1.1)
Fiducial	Track fiducial to CES
Track P_T	$\geq$ 10 or $\geq$ 5 if E_T <20 (GeV)
Track $\|z_0\|$	$\leq$60 cm.
# of Axial SL	$\geq$3 with $\geq$5 hits
# of Stereo SL	$\geq$2 with $\geq$5 hits
Conversion Flag	$\neq$1
Isolation/E_T	$\leq$ 0.1
E_{HAD}/E_{EM}	<0.055+0.00045 $\cdot$ E
L_{shr}	$\leq$0.2
E/P	<0.055+0.00045$\cdot$ E_t
CES ΔX	-3 $\leq$ q $\cdot$ ΔX $\leq$ 1.5

Forward Electrons (PHX)	
Region	Plug (1.2< $\|\eta\|$ <2.0)
η_{PES}	(1.2< $\|\eta\|$ <2.0)
E_{HAD}/E_{EM}	<0.05
PEM 3x3 Fit	true
$\chi^2_P ES$	$\leq$ 10
PES 5x9 U	$\geq$ 0.65
PES 5x9 V	$\geq$ 0.65
Isolation/E_T	$\leq$ 0.1
ΔR(PES,PEM)	$\leq$3.0
Track Method	true
# of Silicon Hits	$\geq$3 hits
Track $\|z_0\|$	$\leq$60 cm.

Table 3: Electron Identification Requirements

Three muon categories are used in this analysis: CMUP, CMX, and CMIOCES. There are certain base requirements that all muons must fulfill, which are listed in Table 4. Also, muons are further designated by the specific detector through which they pass. CMUP muons must have a stub in both the CMU detector as well as in the CMP muon chambers. The pseudo-rapidity range accounted for is η_{det} <0.68. CMX muons must have a stub in the CMX detector, which covers the range 0.68< η_{det} <1. It is also possible to identify muons not fiducial to these detectors by identifying a high-P_T track that points to a calorimeter with that of a minimizing ionizing particle. We call these CMIOCES muons and these include tracks that have only a CMU stub or only a CMP stub. Additional requirements for the different muons types (in addition

Central Muons	
P_T	>20 GeV)
E_{EM}	<2+max(0,(p-100)·0.0115)
E_{HAD}	<6+max(0,(p-100)·0.028)
Isolation/P_T	≤0.1
# of Axial SL	≥3 with ≥5 hits
# of Stereo SL	≥2 with ≥5 hits
Track z_0	<60 cm.
Track d_0	<0.2 cm. (<0.02 cm. with silicon)
χ^2/dof	<4.0 cm. (<3.0 cm. if Run>186598)

Table 4: Identification requirements for all muon types.

CMUP Muon	
CMU Fiducial	x_{fid} <0,z_{fid} <0 cm
CMP Fiducial	x_{fid} <0,z_{fid} <0 cm
ΔX_{CMU}	< 7cm
ΔX_{CMP}	< max(6,150/P_T) cm

CMX Muon	
CMX Fiducial	x_{fid} <0,z_{fid} <0 cm
ΔX_{CMX}	< max(6,125/P_T) cm
ρ_{COT}	> 140 cm

CMIOCES Muon	
Uniqueness	Not a CMUP or CMX
$E_{EM} + E_{Had}$	>0.1 GeV
# of Stereo SL	≥2 with ≥5 hits
Fiducial	Track fiducial to PES
COT hit fraction	>0.6
χ^2/dof	< 3.0

Table 5: Additional identification requirements for the three muon types used in this analysis.

to the base cuts) are given in Table 2.3.

2.4 Dilepton Selection

The sample we fit consists of two oppositely charged leptons (electrons or muons) isolated from other activity in the event. Table 6 lists the requirements we make on the sample to select $e\mu$ events that we then fit in the $\not\!\!E_T$-N_{jet} and $\not\!\!E_T$-$\sum E_T(jets)$ parameter spaces.

Event Selection Cuts
1 high-E_T (>20 GeV) isolated electron + 1 high-P_T (>20 GeV) isolated muon
Apply cosmic filter
Apply conversion filter
Require that the electron and muon be of opposite sign

Table 6: Selection requirements of $e\mu$ events used in this analysis.

Process	Acceptance	Expected Number of $e\mu$ Events in 3.0fb^{-1}
$t\bar{t}$	(0.510 ± 0.002) %	82.4 ± 0.3
WW	(0.431 ± 0.002)% %	128.0 ± 0.6
$Z \to \tau\tau$	(0.0480 ±.0003) %	470.6 ± 3.4

Table 7: Signal Process Acceptances (including branching ratios to $e\mu$ final state) and expected numbers of events. Errors are statistical only.

The $e\mu$ categories we consider are: TCE-CMUP, TCE-CMX, TCE-CMIOCES, PHX-CMUP, and PHX-CMX.

3 Signal and Background acceptances

The acceptances for our signal processes ($t\bar{t}$, WW, $Z \to \tau\tau$) are summarised in Table 7. The errors are statistical only from the Monte Carlo samples we used. These acceptances include the branching ratios of the processes to decay to our $e\mu$ categories.

The backgrounds we consider are Drell-Yan ($Z/\gamma \to ee,\ \mu\mu$), WZ, ZZ, $b\bar{b}$, $W\gamma$ and $W+$ fake lepton, where the fake lepton is a jet which has been mistakenly identified as a lepton. These contributions are typically much smaller than our our signal samples from the previous section, and in all our fits we fix these to their expected values.

Our fake background is data driven and estimated by first determining the probability for a jet to fake an electron or muon. We then apply these fake rates to our $W + jet$ data samples, and apply all other analysis cuts, to establish the contribution from this background. This procedure and all the relevant plots and results is detailed in CDF-9697 [3]. All other backgrounds are determined from Monte Carlo (samples given in section 2.2).

A summary of the numbers of "background" events expected after the requirement of an isolated electron and muon is given in Table 4.

	$e\mu$ Final State
Signal Processes	
$t\bar{t}$	82.4 ± 10.4
WW	128.0 ± 16.2
$Z \to \tau\tau$	470.6 ± 40.9
Background Processes	
$DY \to ee$	0.19 ± 0.02
$DY \to \mu\mu$	103 ± 18
WZ	4.6 ± 0.6
ZZ	1.0 ± 0.1
$W\gamma$	12.0 ± 1.6
$W + jet$	52.5 ± 21.3
Total expected MC Event Count	854 ± 88
Data	781

Table 8: Grand summary of the numbers of expected events for all processes used in this analysis. Errors are include both statistical and systematic uncertainties. The integrated luminosity used is about $3.0\,\mathrm{fb}^{-1}$

4 Data and grand summary of expectations

Table 4 shows the summary of all the signal and background expectations discussed in the previous sections. The luminosity normalised to for each process depends slightly on that process but on average is $184 \pm 11\,\mathrm{pb}^{-1}$. The errors include statistical and systematics on the acceptances. Also shown are the number of observed events in each channel from our data samples.

5 Parameter space distributions for data and MC

The $\not\!\!E_T$-N_{jet} and $\not\!\!E_T$-$\sum E_T(jets)$ 2-D parameter space distributions for the expected signal processes, and the "fixed" total background are shown in Figures **??**. These define the shapes that are fit to the corresponding data distribution in Figure 6 for the cross section extractions of the signal processes.

Shown in Figure 7 are the $\not\!\!E_T$ distributions for the different jet multiplicities, comparing the expectated distributions to those observed in data. The expected distributions are derived from the templates in Figures **??** normalized to the expected numbers in Table 4.

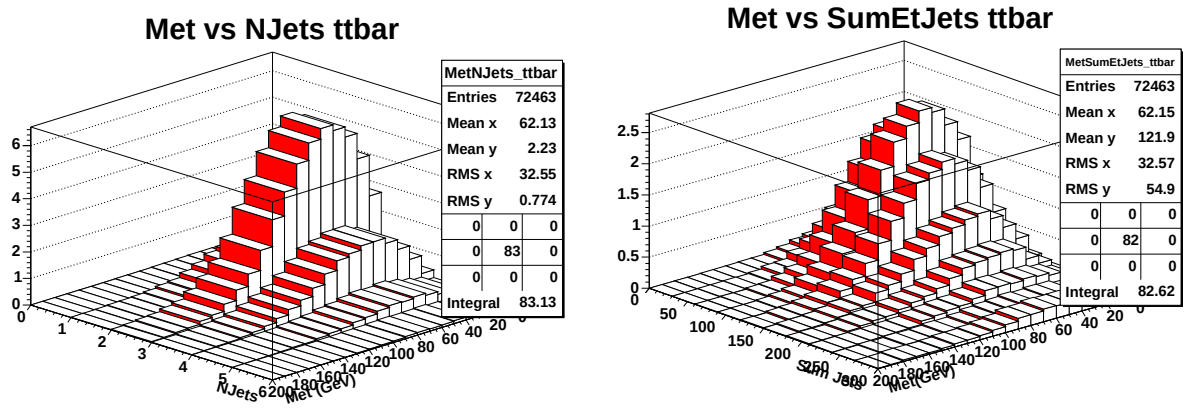

Figure 2: The $\not\!\!E_T$-N_{jet} (left) and $\not\!\!E_T$-$\sum E_T(jets)$ (right) expected distributions for $t\bar{t}$.

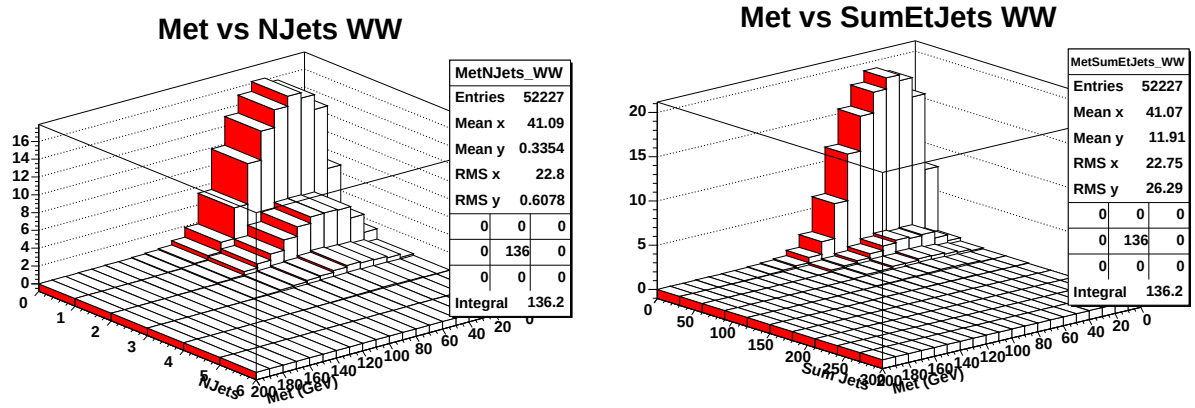

Figure 3: The $\not\!\!E_T$-N_{jet} (left) and $\not\!\!E_T$-$\sum E_T(jets)$ (right) expected distributions for WW.

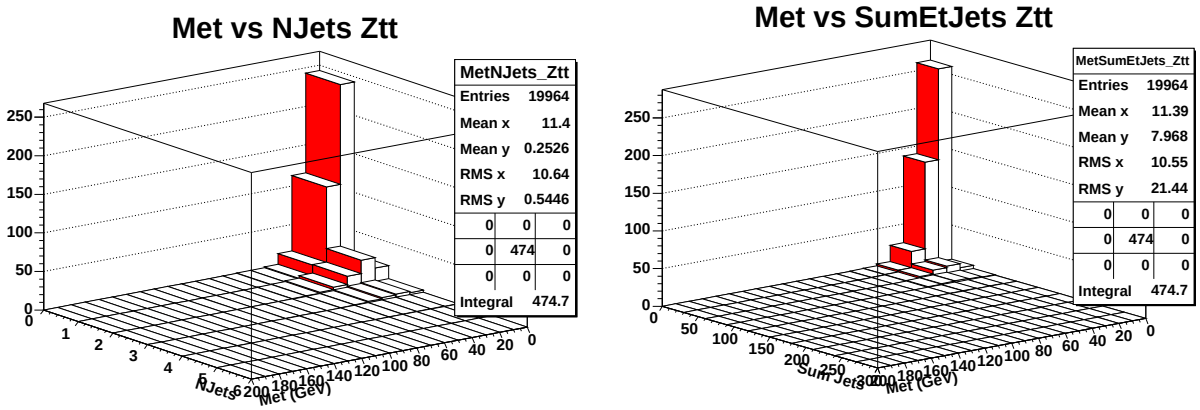

Figure 4: The $\not\!\!E_T$-N_{jet} (left) and $\not\!\!E_T$-$\sum E_T(jets)$ (right) expected distributions for $Z/\gamma^* \to \tau\tau$.

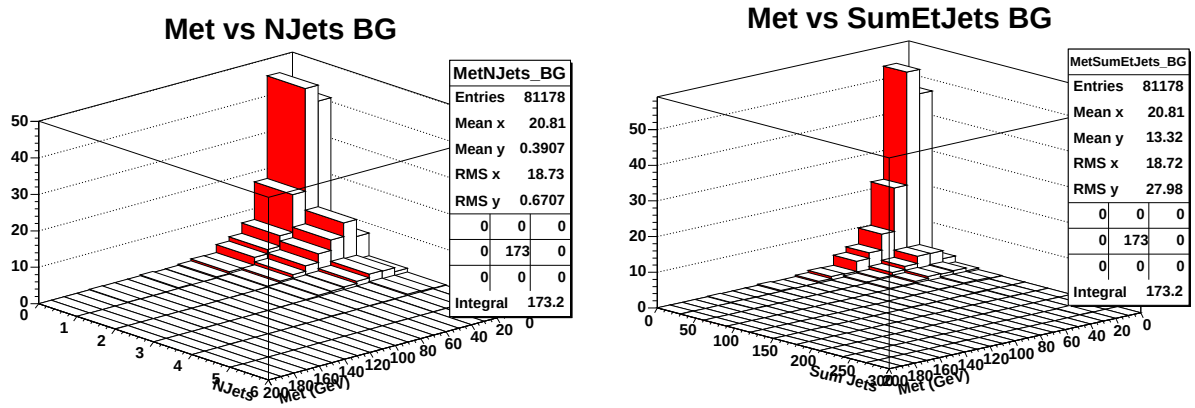

Figure 5: The $\not\!\!E_T$-N_{jet} (left) and $\not\!\!E_T$-$\sum E_T(jets)$ (right) expected distributions for the combined backgrounds (see text).

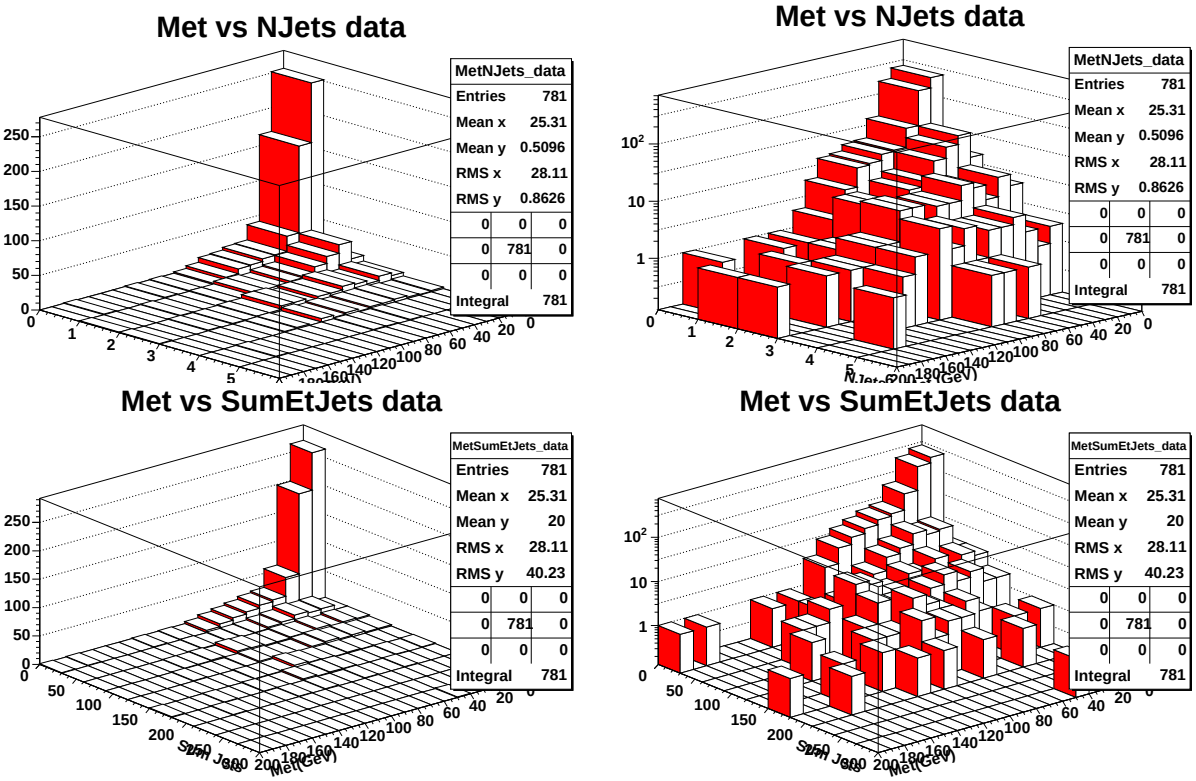

Figure 6: The $\not\!\!E_T$-N_{jet} (top) and $\not\!\!E_T$-$\sum E_T(jets)$ (bottom) distributions observed in 3.0fb^{-1} of data. Also shown are the distributions in log scale to make the low statistics bins more observable.

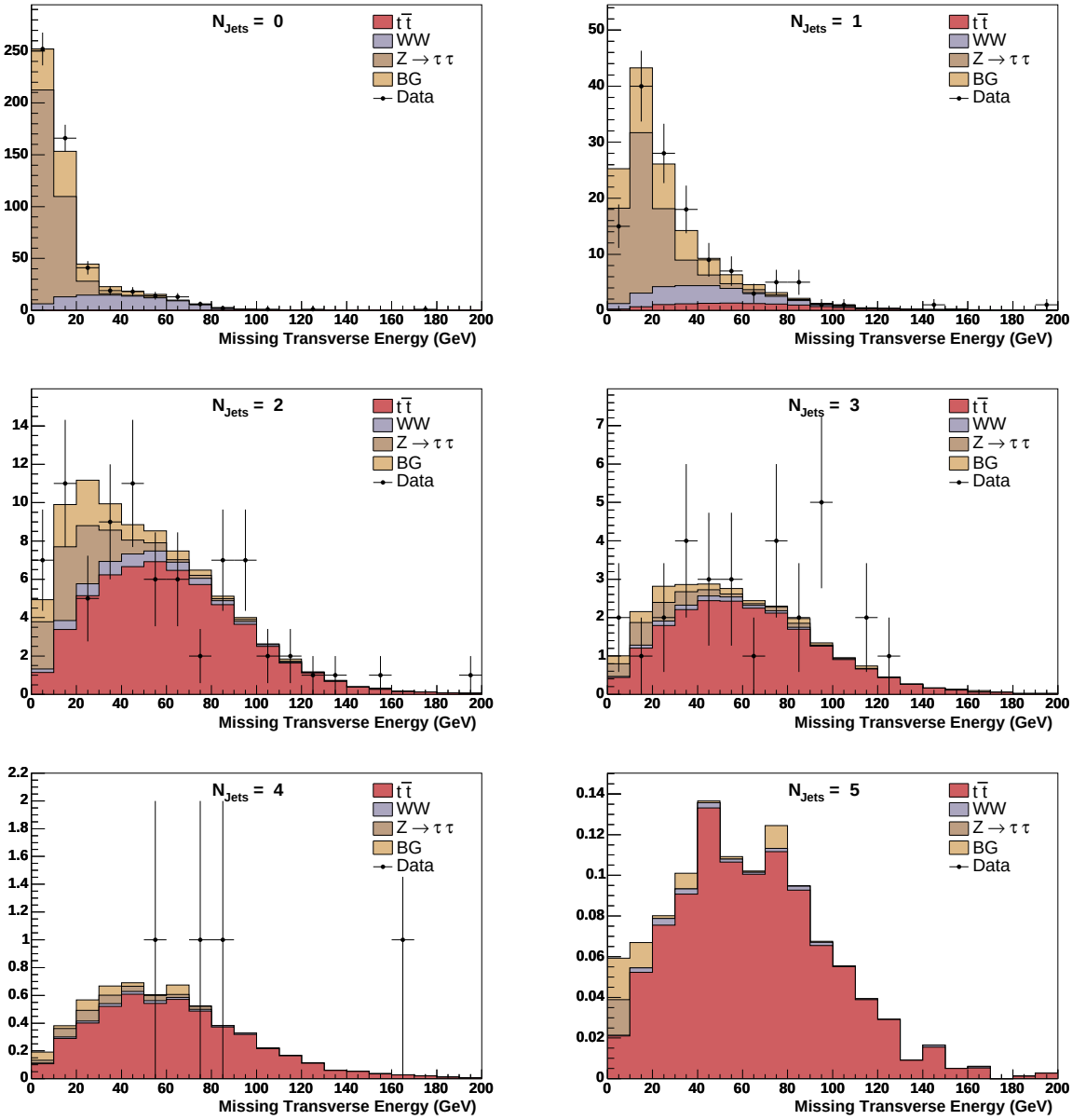

Figure 7: Distributions of $\not\!\!E_T$ for various jet multiplicities, comparing expectations to data. The expected distributions are normalized to their expected numbers given in Table 4.

6 The Likelihood fit technique

We form a Likelihood function from the Poisson probabilities comparing each bin in the $\not\!\!E_T$-N_{jet} space of the data with that of all the SM contributions, with Gaussian terms to constrain the nuisance parameters (acceptances, luminosity) within their estimated systematic uncertainties. We minimize the negative of the logarithm of this Likelihood function using the CERN package MINUIT [5], as described below.

A binned maximum likelihood method is used to extract the WW, $t\bar{t}$, and $Z \to \tau\tau$ cross sections using the shape of the 2D $\not\!\!E_T$-N_{jet} (or $\not\!\!E_T$-$\sum E_T$ of jets) distributions from signal and background along with their estimated normalizations and systematic uncertainties. The best fit to these distributions, or the maximum likelihood, gives the best measure of these cross section.

The likelihood function is formed from a product of Poisson probabilities for each bin in in the 2D distribution. Additionally, Gaussian constraints are applied corresponding to each systematic S_c. The likelihood is given by

$$\mathcal{L} = \left(\prod_i \frac{\mu_i^{n_i} e^{-\mu_i}}{n_i!} \right) \cdot \prod_c e^{\frac{S_c^2}{2}} \tag{1}$$

where μ_i is the total expectation in the i-th bin and n_i is the number of data events in the i-th bin. μ_i is given by

$$\mu_i = \sum_k \alpha_k \left[\prod_c (1 + f_k^c S_c) \right] (N_k^{Exp})_i \tag{2}$$

Here f_k^c is the fractional uncertainty associated with the systematic S_c and process k. This is constructed such that the systematics are properly correlated (or uncorrelated) between the different contributions[2]. This follows the procedure outlined in reference [6]. $(N_k^{Exp})_i$ is the expected number of events from process k in the i-th bin. α_k is the parameter which is used to measure the cross section(s) of interest. It is a freely floating parameter for cross sections we wish to measure. In this sense it allows one to measure an additional overall normalization on these processes which is then interpreted as the multiplicitave factor by which you would get from the input (usually theoretical) cross section, to the actual measured cross section, for example

$$\sigma_{WW}^{measured} = \alpha_{WW} \cdot \sigma_{WW}^{NLO}.$$

We minimize the negative of the logarithm of this Likelihood function using the CERN package MINUIT [5]. The errors used in this analysis are the asymmetric errors returned by MINOS.

[2]Note that if a systematic is partially correlated it is possible to decompose that into its correlated and uncorrelated parts

6.1 Pseudo-experiments

In order to quantify our expectations 10,000 pseudo-experiments are generated, each of which is treated exactly as data would be in the minimization. In generating pseudo-experiments, care has been taken to ensure that variations of the systematic parameters (S_c) are correctly correlated (or uncorrelated) between processes. This is done in the following way:

- Construct an array of Gaussianly distributed numbers g_c
- Fluctuate the nominal prediction (N_k^{Exp}) for each process k according to their fractional uncertainties (f_k^c) and the systematic fluctuations (g_c) such that the new "Gaussianly" fluctuated number is

$$G_k = N_k^{Exp} \prod_c (1 + f_k^c g_c).$$

- Poisson fluctuate the resulting number:

$$P_k = \text{Poisson}(G_k).$$

P_k is then the number of events which will be drawn at random from process k (the LR_{WW} template for process k) with a probability according to its distribution. Figures **??** summarize the results of these pseudo-experiments for various floating parameters α_k. The full set of systematics are included which are discussed in section 7. In addition, the pull distributions from the $\not\!\!E_T$-N_{jet} fits with all signal processes floating are given in Figure 10.

Based on these pseudo-experiment results, we see no great gain in using $\not\!\!E_T$-$\sum E_T(jets)$ instead of $\not\!\!E_T$-N_{jet}, so our main results will use the $\not\!\!E_T$-N_{jet} fits, but with the $\not\!\!E_T$-$\sum E_T(jets)$ results still carried out for use as a cross-check.

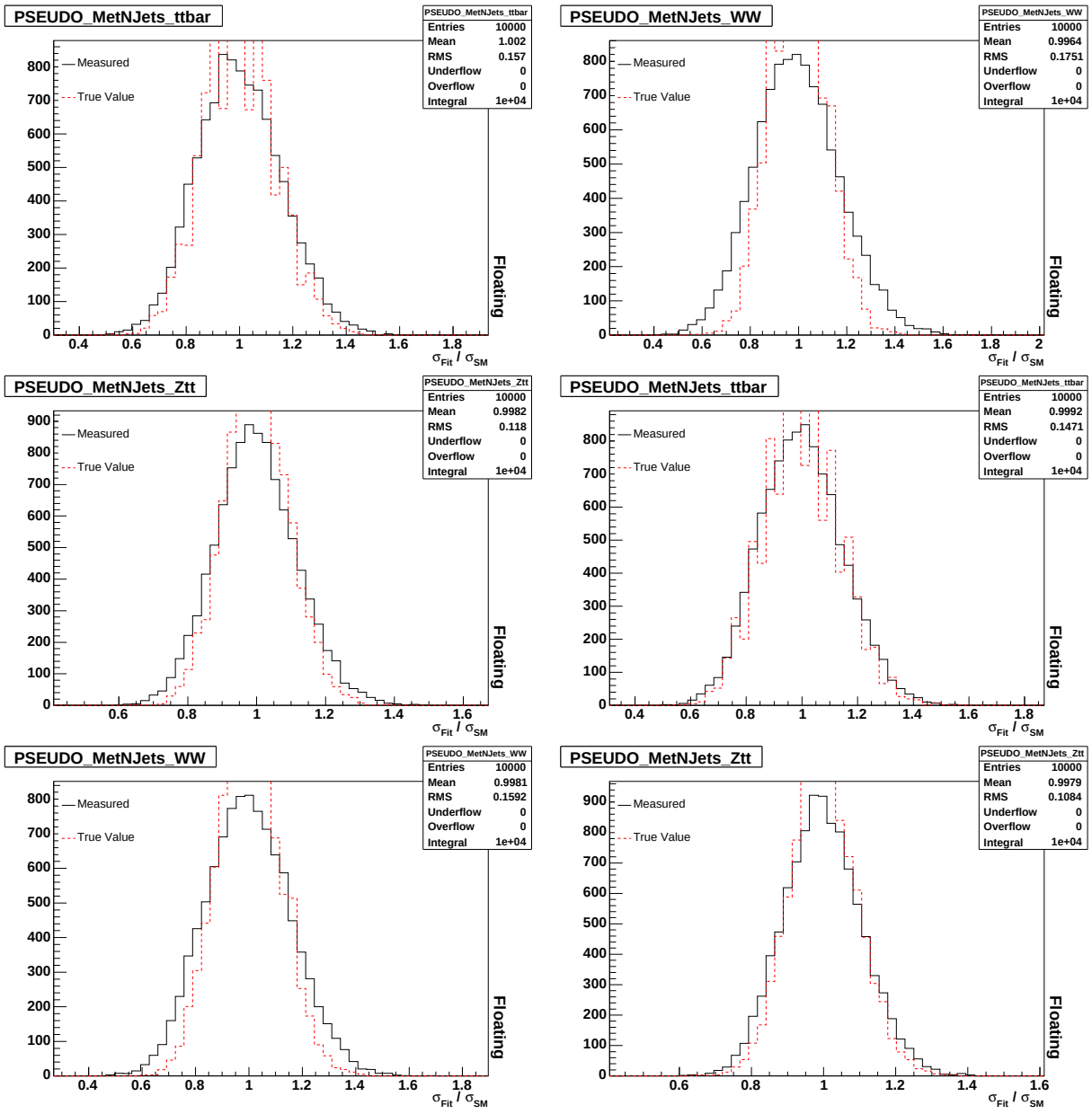

Figure 8: Cross section ratios from pseudo-experiment fits to the $\not\!\!E_T$-N_{jet} parameter space (solid histogram). The dashed histogram is the input distribution. The fitted pseudo-experiment cross sections are given as ratios to 6.7 pb for $t\bar{t}$, 12.4 pb for WW, and 1780.8 pb for $Z \to \tau\tau$. The plots refer to the following scenarios (left to right, top to bottom): $\sigma_{t\bar{t}}$ for all signal processes floating, σ_{WW} for all signal processes floating, $\sigma_{Z\to\tau\tau}$ for all signal processes floating, $\sigma_{t\bar{t}}$ for all but $t\bar{t}$ "fixed", σ_{WW} for all but WW "fixed", $\sigma_{Z\to\tau\tau}$ for all but $Z \to \tau\tau$ "fixed".

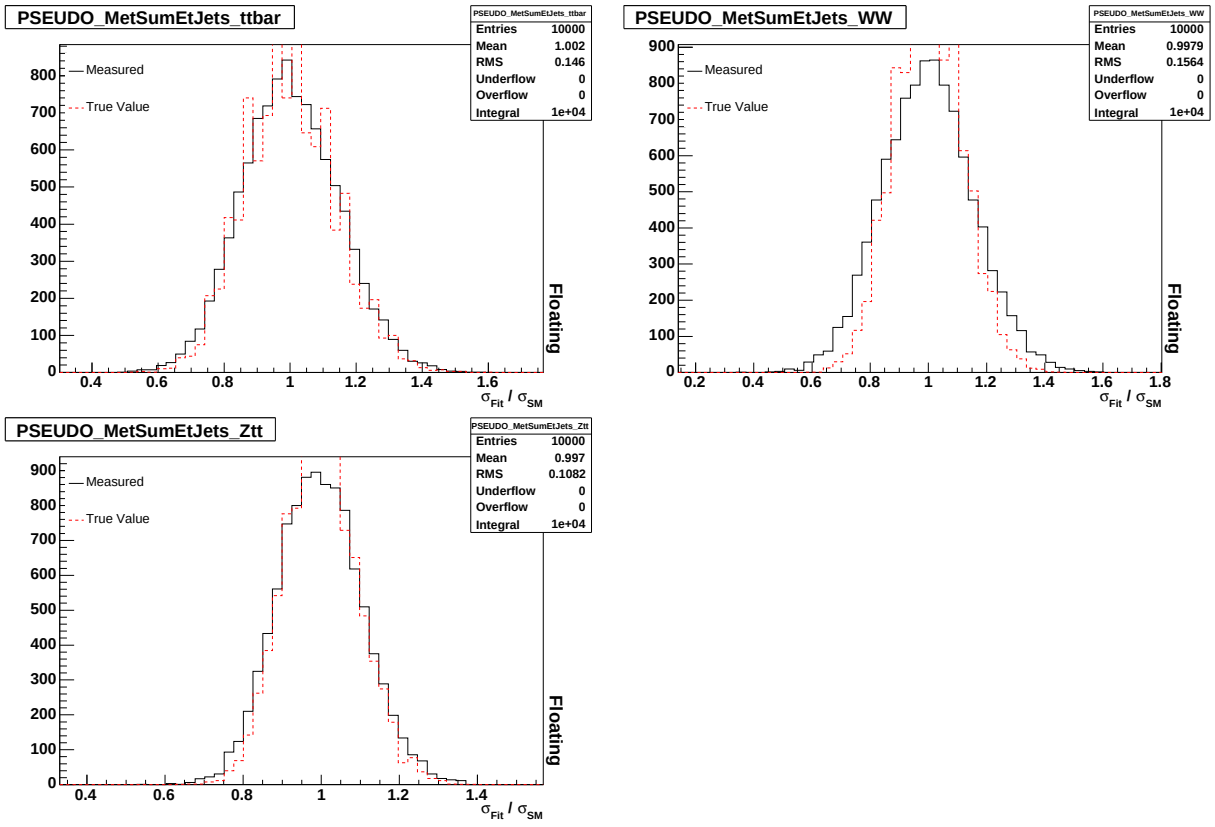

Figure 9: Cross section ratios from pseudo-experiment fits to the $\not\!\!E_T$-$\sum E_T(jets)$ parameter space (solid histogram). The dashed histogram is the input distribution. The fitted pseudo-experiment cross sections are given as ratios to 6.7 pb for $t\bar{t}$, 12.4 pb for WW, and 1780.8 pb for $Z \rightarrow \tau\tau$. The plots refer to the following scenarios (left to right, top to bottom): $\sigma_{t\bar{t}}$ for all but $t\bar{t}$ "fixed", σ_{WW} for all but WW "fixed", $\sigma_{Z\rightarrow\tau\tau}$ for all but $Z \rightarrow \tau\tau$ "fixed".

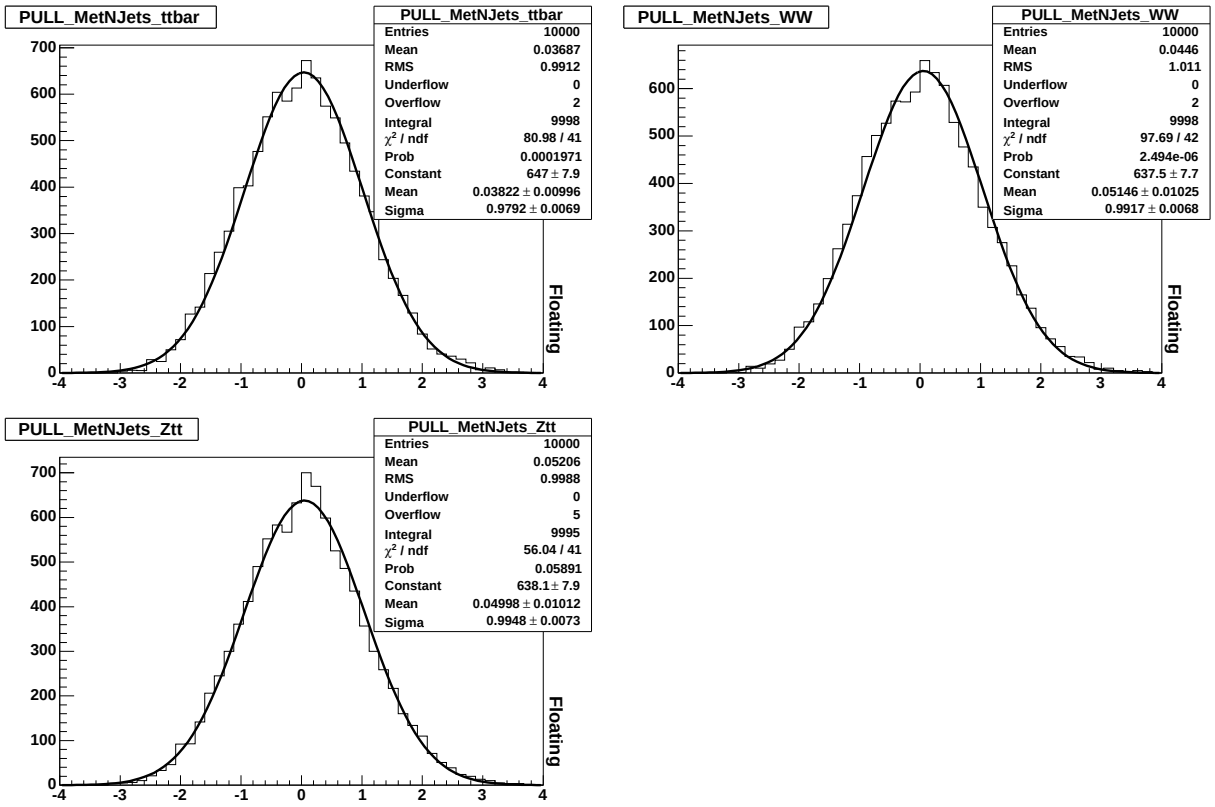

Figure 10: Pull distributions from pseudo-experiment cross section fits to the $\not\!\!E_T$-N_{jet} parameter space. The pull distributions are from the fit with all signal processes floating, for $t\bar{t}$, WW, and $Z \rightarrow \tau\tau$, respectively.

7 Systematics

We have two classes of systematics that we treat differently in our analysis, one, the systematic uncertainty (from various sources) on the acceptances themselves, and a second due to the effect on the fitted cross sections from changes in the $\not\!\!E_T$-N_{jet} shapes due to various sources. The following 2 subsections give a brief overview of our two systematic sources.

7.1 Acceptance systematics

A summary of our acceptance systematics is given in Table 7.1. We incorporate these systematics in our fit by allowing the acceptances to vary in the likelihood function within a Gaussian constraint (of width given by the systematic error) as discussed in section 6. In addition, although not explicitly mentioned above, we have a similar Gaussian constraint for the luminosity (of width 6%). More details of the systematics considered can be found in CDF-9697 [3].

	$t\bar{t}$	WW	$Z \to \tau\tau$
Lepton ID	1.9 %	1.9 %	1.9 %
Trigger Eff.	2.1 %	2.2 %	3.5 %
MC Dependence	4.1 %	3.5 %	–
Process Cross Section	10.0 %	10.0 %	5.0 %

Table 9: Summary of systematic uncertainties on the acceptance for each "signal" process.

	$Z \to ee$	$Z \to \mu\mu$	ZZ	WZ	$W\gamma$	$W + jets$
lepton ID	1.9 %	1.9 %	1.9 %	1.9 %	1.9 %	1.9 %
Trigger Eff.	3.5 %	3.5 %	3.5 %	3.5 %	3.5 %	3.5 %
Process Cross Section	5.0 %	5.0 %	10.0 %	10.0 %	10.0 %	–
Fakes	–	–	–	–	–	28.6 %

Table 10: Summary of systematic uncertainties on the acceptance for each "background" process.

7.2 Shape systematics

We have investigated the effect of sources of uncertainties on the shapes of the $\not\!\!E_T$-N_{jet} distributions. These include; Jet Energy scale, ISR and FSR, and the effect of different bin sizes.

- **Jet Energy Scale :** Using pseudo-experiments sampled from templates created from increasing and decreasing the jet energies by 10% (a gross overestimate of our JES systematic), we found the effect on the expected cross sections to vary by about 2% for WW and $Z \to \tau\tau$, and about 5% for $t\bar{t}$. Given that the actual JES systematic varies between about 2% and 3% the shape systematic due to this effect is probably a couple of percent at most.

- **ISR/FSR :** To estimate this effect we used standard samples of more/less ISR/FSR. In all cases the effect on the cross sections was around 2% or less. This effect will also be correlated to the JES effect.

- **Bin size:** To estimate the effect of bin size, we halved the bin size (doubled the number of bins) in the $\not\!\!E_T$-N_{jet} fits. The effect on the mean cross section from pseudoexperiments was negligible (less than 1%).

The conclusion is that these effects are small compared to our acceptance systematics, the total being of order 3% (as an upper limit) for all signal processes. We therefore do not include a separate shape systematic in our quoted results.

8 Fit results

We fit the data to our SM signal templates using the scenarios discussed earlier and which are all summarized in Tables 11.

	$e\mu$	Theory
$\not\!\!E_T$ vs. N_{jets}		
$\sigma(t\bar{t})$ (WW and $Z \to \tau\tau$ Constrained) (pb)	$8.20^{+1.04}_{-0.98}(\text{stat.})^{+0.54}_{-0.43}(\text{syst.})$ pb	6.7 ± 0.3
$\sigma(t\bar{t})$ (pb) (all floating)	$7.81^{+0.99}_{-0.93}(\text{stat.})^{+0.71}_{-0.55}(\text{syst.})$ pb	
$\sigma(WW)$ ($t\bar{t}$ and $Z \to \tau\tau$ Fixed) (pb)	$12.28^{+1.75}_{-1.65}(\text{stat.})^{+1.07}_{-0.88}(\text{syst.})$ pb	12.4 ± 0.8
$\sigma(WW)$ (pb) (all floating)	$11.66^{+1.46}_{-1.37}(\text{stat.})^{+1.65}_{-1.42}(\text{syst.})$ pb	
$\sigma(Z \to \tau\tau)$ ($t\bar{t}$ and WW Fixed) (pb)	$1513\ ^{+94}_{-91}(\text{stat.})^{+145}_{-130}(\text{syst.})$ pb	1781 pb
$\sigma(Z \to \tau\tau)$ (pb) (all floating)	$1542^{+97}_{-95}(\text{stat.})^{+175}_{-154}(\text{syst.})$ pb	
$\not\!\!E_T$ vs. $\sum E_T$(jets)		
$\sigma(t\bar{t})$ (WW and $Z \to \tau\tau$ Constrained) (pb)	$7.41^{+1.02}_{-0.95}(\text{stat.})^{+0.41}_{-0.34}(\text{syst.})$ pb	6.7 ± 0.3 pb
$\sigma(t\bar{t})$ (pb) (all floating)	$6.70^{+0.91}_{-0.85}(\text{stat.})^{+0.64}_{-0.51}(\text{syst.})$ pb	
$\sigma(WW)$ ($t\bar{t}$ and $Z \to \tau\tau$ Fixed) (pb)	$13.19^{+1.84}_{-1.73}(\text{stat.})^{+1.13}_{-0.94}(\text{syst.})$ pb	12.4 ± 0.8 pb
$\sigma(WW)$ (pb) (all floating)	$11.87^{+1.62}_{-1.53}(\text{stat.})^{+1.58}_{-1.32}(\text{syst.})$ pb	
$\sigma(Z \to \tau\tau)$ ($t\bar{t}$ and WW Fixed) (pb)	$1464^{+91}_{-88}(\text{stat.})^{+145}_{-130}(\text{syst.})$ pb	1781 ± 90 pb
$\sigma(Z \to \tau\tau)$ (pb) (all floating)	$1451^{+92}_{-90}(\text{stat.})^{+172}_{-152}(\text{syst.})$ pb	

Table 11: Cross-section measurements from various data fit scenarios, for 3.0 fb^{-1} of data. For each channel, we extract two sets of values: either all the cross-sections are left unconstrained, or two are fixed to their SM expectations.

9 Likelihood of Standard Model hypothesis

The fit results from section 8 to the entire parameter space(s) yield likelihood values consistent with that from pseudo-experiments. This are shown in Figures 11 and 12.

However, this is not necessarily a very good measure of the consistency to the SM as it might not be sensitive to significant variations in regions with relatively low statistics. We therefore split the $\not\!\!E_T$-N_{jet} parameter space into 4 regions like so (we do this only for the $\not\!\!E_T$-N_{jet} parameter space as these represent our main results):

- region 1: $met < 20GeV$, $N_jets \leq 1$
- region 2: $met > 20GeV$, $N_jets \leq 1$
- region 3: $met > 20GeV$, $N_jets \geq 2$
- region 4: $met < 20GeV$, $N_jets \geq 2$

Table 12 summarizes the results from comparing the likelihood from the data to pseudo-experiments in each of these regions. The corresponding likelihood plots are given in Figure 13.

Region 1	86.7%
Region 2	25.1%
Region 3	24.8%
Region 4	32.2%

Table 12: Percentage of pseudo-experiments with a likelihood greater than that from the fit to the data for each of the 4 regions in the $\not\!\!E_T$-N_{jet} parameter space. The fit is that with all three signal processes floating.

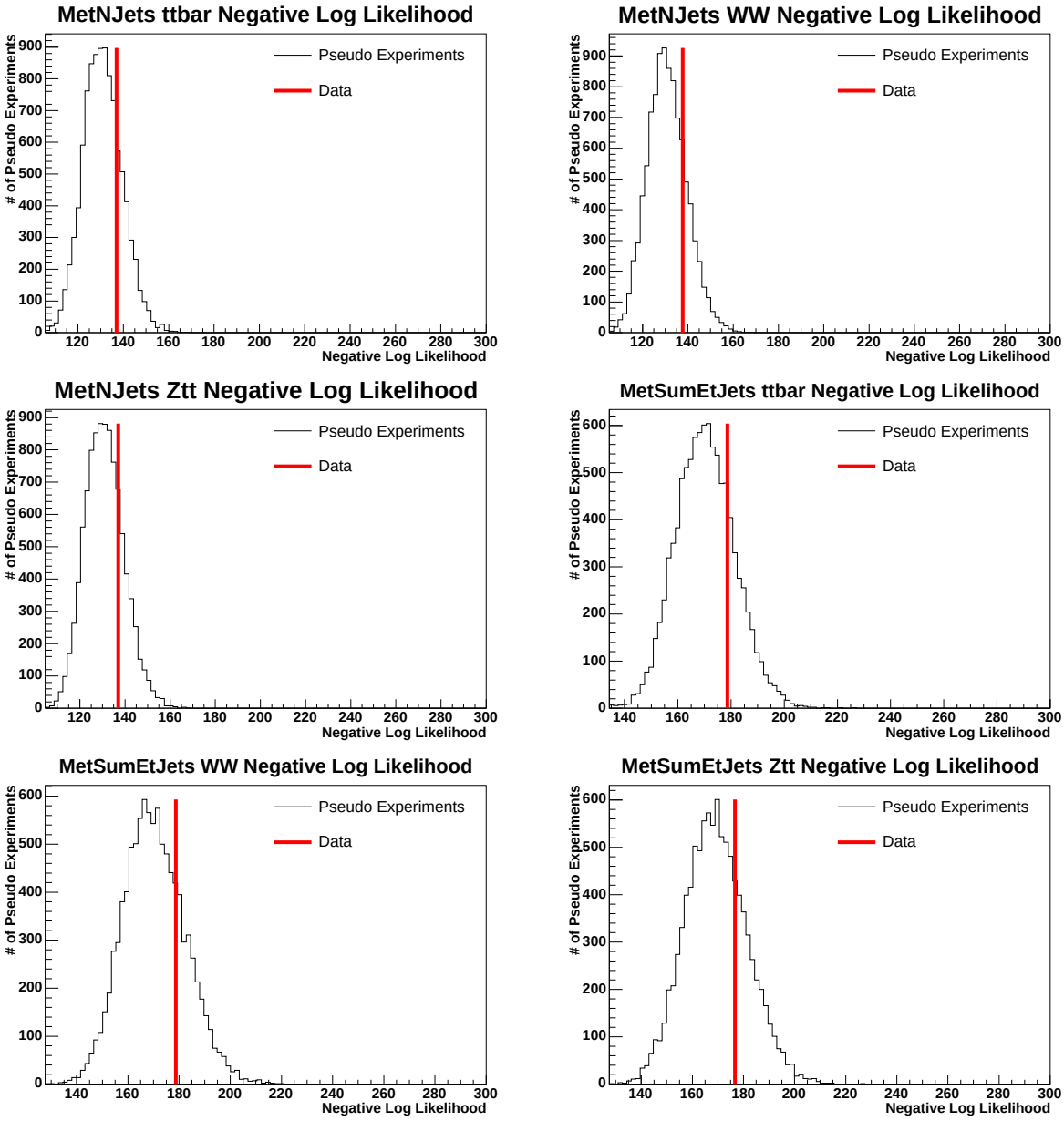

Figure 11: Negative log-likelihood values from fits to the data (solid red line) as compared to the distributions from pseudo-experiments. These correspond to the fits where all but the measured process is constrained in the fit, for fits using the both the $\not\!\!E_T$-N_{jet} and $\not\!\!E_T$-$\sum E_T(jets)$ parameter spaces.

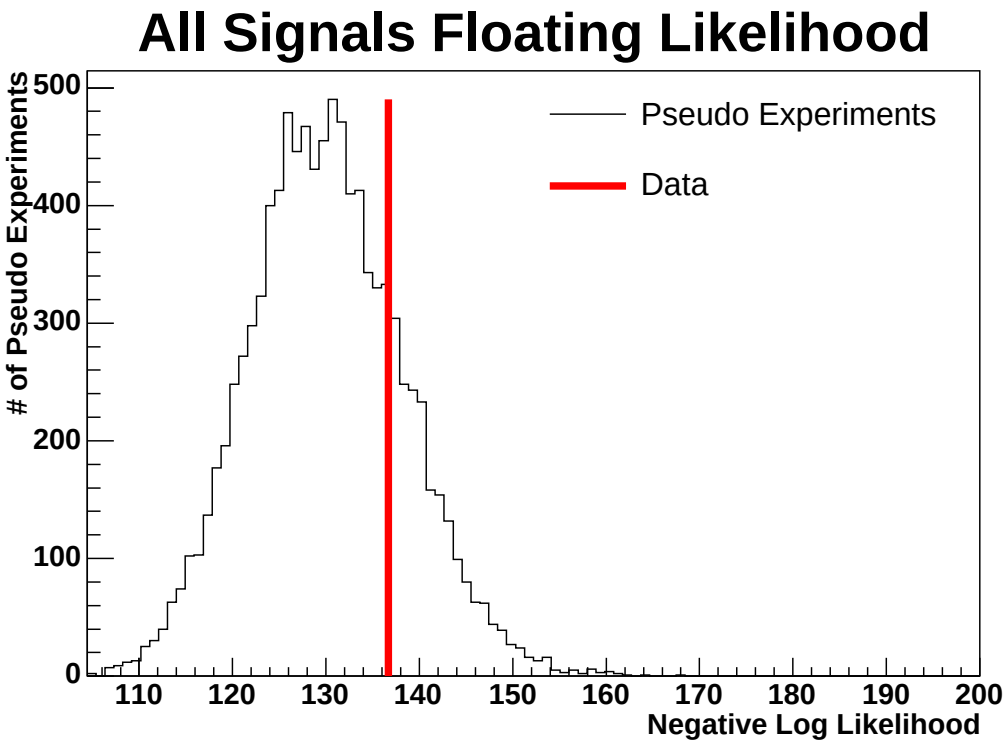

Figure 12: Negative log-likelihood value from the $\not\!\!E_T$-N_{jet} fit to the data with all signal processes floating (solid red line) as compared to the distribution from pseudo-experiments.

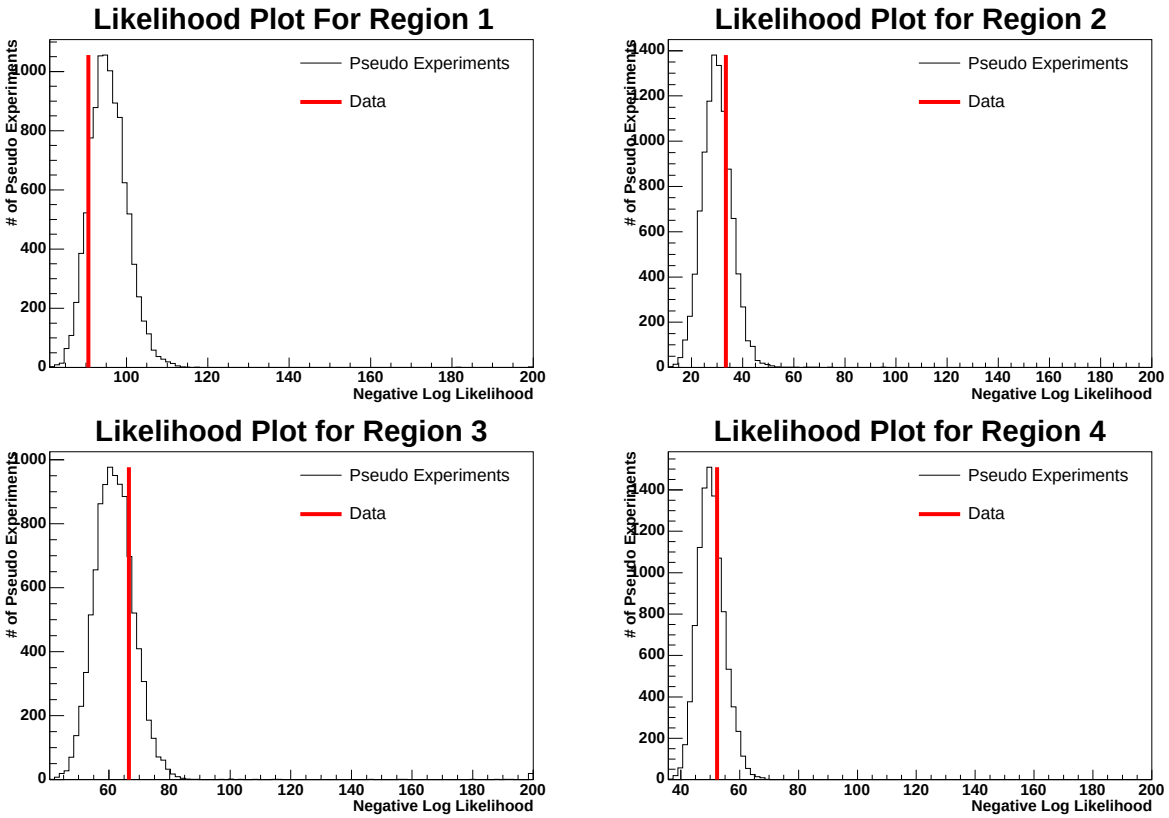

Figure 13: Negative log-likelihood values from the $\not\!\!E_T$-N_{jet} fits to the data with all signal processes floating (solid red line) as compared to the distributions from pseudo-experiments, for the four regions discussed in the text.

10 Summary and possible future improvements

We have taken the $e\mu$ events from the $H \rightarrow WW$ analysis to use in an analysis technique for simultaneously measuring the $t\bar{t}$, WW, and $Z \rightarrow \tau\tau$ cross sections, orginally documented and published in reference [2, 1]. This analysis gives us a more global test of the SM using dilepton events than a dedicated cross section measurement, and we quantify the consistency of our data in various regions of the $\not\!\!E_T$-N_{jet} parameter space.

This could be used for more specific searches for new physics, and we plan on developing this using same-sign dileptons events, and as a tool for looking at early LHC data. In addition, to gain better separation for $Z \rightarrow \tau\tau$ and perhaps use as a tool in $H \rightarrow \tau\tau$ searches, we plan to investigate the use of a third axis of "visible mass" (this is in fact being done for a prototype ATLAS analysis).

References

[1] A. Abulencia *et al.* (CDF collaboration), "Cross Section Measurements of High-p_T Dilepton Final-State Processes Using a Global Fitting Method", Phys. Rev. D78, 012003 (2008).

[2] S. Carron, D. Benjamin, M. Coca, M. Kruse, "A global analysis of the high-P_T dilepton sample using 200 pb^{-1} of Run 2 data", CDF-note 6870.

[3] CDF-9697, "Updated search for H to WW Production Using 3.6 fb-1"

A. Abulencia *et al.* (CDF collaboration), "Search for Higgs Bosons decaying to pairs of W-Bosons", Phys. Rev. Lett. 102, 021802 (2009). arXiv:0809.3930

[4] Baur, U. and Berger, E. L., Phys. Rev. D47 (1993) 4889-4904.

[5] F. James, Minuit Reference Manual, Version 94.1 http://wwwasdoc.web.cern.ch/wwwasdoc/WWW/minuit/minmain/minmain.html.

[6] CDF-8128, Tom Junk